Journal of Power Sources 237 (2013) 156–166

Contents lists available at SciVerse ScienceDirect

Journal of Power Sources

journal homepage: www.elsevier.com/locate/jpowsour

Carbonaceous nickel oxide nano-composites: As electrode materials in electrochemical capacitor applications

Anirudha Jena [a], N. Munichandraiah [b], S.A. Shivashankar [a,c,*]

[a] Materials Research Centre, Indian Institute of Science, Bangalore 560012, India
[b] Department of Inorganic and Physical Chemistry, Indian Institute of Science, Bangalore 560012, India
[c] Centre for Nano Science and Engineering, Indian Institute of Science, Bangalore 560012, India

HIGHLIGHTS

- Solution based microwave process is used to synthesize nano-composites of NiO.
- Adducted metal organic complex is used as a single source precursor for synthesis of carbonaceous nano-composites.
- By tuning the nature of solvents in the reaction medium it is possible to obtain either NiO/C or Ni/NiO/C composite.
- These composites show superior performance as electrode material for supercapacitor applications.
- Nano-composite such as Ni/NiO/C show enhanced capacitive behavior for its better conductivity because of C and Ni.

GRAPHICAL ABSTRACT

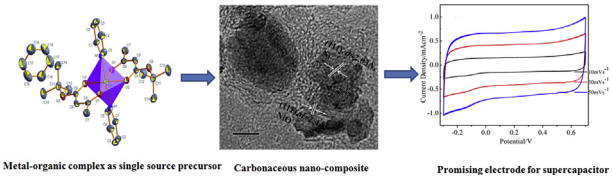

ARTICLE INFO

Article history:
Received 10 January 2013
Received in revised form
7 March 2013
Accepted 9 March 2013
Available online 19 March 2013

Keywords:
Microwave
Nickel/nickel oxide carbonaceous composite
Supercapacitor
Metalorganic complex

ABSTRACT

Carbonaceous nickel oxide powder samples have been synthesized from an adducted nickel β-ketoester complex used as a "single source precursor" through a solution-based microwave-assisted chemical route. Comprehensive analysis of the resulting powder material has been carried out using various characterization techniques. These analysis reveal that, depending on the solvent used, either NiO/C or Ni/NiO/C composites are formed, wherein Ni and/or NiO nanocrystals are enveloped in amorphous carbon. As the components emerge from the same molecular source, the composites are homogeneous on a fine scale, making them promising electrode materials for supercapacitors. Electrochemical capacitive behavior of these oxide composites is studied in a three-electrode configuration. With a specific capacitance of 113 F g^{-1}, Ni/NiO/C is superior to NiO/C as capacitor electrode material, in 0.1 M Na_2SO_4 electrolyte. This is confirmed by impedance measurements, which show that charge-transfer resistance and equivalent series resistance are lower in Ni/NiO/C than in NiO/C, presumably because of the presence of metallic nickel in the former. The cyclic voltammograms are nearly rectangular and the electrodes display excellent cyclability in different electrolytes: Na_2SO_4, KOH and $Ca(NO_3)_2{\cdot}4H_2O$. Specific capacitance as high as 143 F g^{-1} is measured in $Ca(NO_3)_2{\cdot}4H_2O$ electrolyte.

* Corresponding author. Materials Research Centre, Indian Institute of Science, Bangalore 560012, India. Tel.: +91 80 2293 2782; fax: +91 80 2360 7316.
E-mail addresses: shivu@mrc.iisc.ernet.in, sa.shivashankar@gmail.com (S.A. Shivashankar).

0378-7753/$ – see front matter © 2013 Elsevier B.V. All rights reserved.
http://dx.doi.org/10.1016/j.jpowsour.2013.03.038

1. Introduction

Nickel oxide (NiO) has generated considerable interest in its utilization as a relatively low-cost, low-toxicity, and environment-friendly material. NiO has been investigated for several important applications, including as a catalyst for CO oxidation, as an electrochromic material, a gas sensor, as well as in the field of solar cells [1–4]. NiO, like other transition metal oxides, is an important electrode material in the field of energy storage, especially in supercapacitors and lithium ion batteries [5–8]. The energy storage capability in supercapacitor arises from the redox process occurring at the electrode/electrolyte interface that results in the pseudocapacitive performance of NiO. NiO, however, has high resistivity, which is a serious drawback for its use as an electrode material in supercapacitors. Hence, it becomes necessary to enhance the electrode conductivity of NiO-based electrode material in order to improve its electrochemical performance. This can be achieved by developing different NiO-containing composites through controlled chemical methods. Such composites can be made of Ni/NiO, NiO/C or Ni/NiO/C [9–13].

Several efforts have been put forward to construct supercapacitors using carbon-based materials, such as carbon nanotubes, activated carbon, carbon fibers, and graphene [14–17]. Decorating the surface of carbon materials with pseudocapacitor materials such as RuO_2, NiO, MnO_2, or conducting polymers, can further enhance their electrochemical performance [18–21]. In particular, the NiO-based composite electrodes of either NiO/C or Ni/NiO/C have exhibited high specific capacitance and good power characteristics attributed to the conducting support for nickel oxide provided by Ni or C. Microwave-assisted chemical route has been used to synthesize composites such as Ni/NiO and NiO/C [22–24].

Although the capacitive property of composite electrodes is better than that of pristine oxide electrodes, the synthesis of the electrode material usually involves a thorough (physical) mixing its components. If, by contrast, a composite such as NiO/C can be synthesized in a single step, from a single chemical source, one may expect that such a composite to be more homogeneous and more effective as an electrode material. Metal-organic complexes, with direct metal–oxygen bonds in their molecular structure as well as carbon, may be expected to be such "single-source" precursors to composite electrode materials. It may even be expected that, by choosing an appropriate metal organic complex and by using it as the precursor in a suitable chemical reaction, the synthesis of composites such as NiO/C and Ni/NiO/C can be achieved, with all the elements derived from the same source. In the latter composition, the percolation of the metal particles through the carbon matrix can reduce the overall electrical resistance of the composite.

In this study, the synthesis of carbonaceous NiO-containing composites via microwave-assisted chemical synthesis in a solution medium, using an adducted nickel β-ketoester complex as precursor has been reported. Present approach focuses on a "single source precursor" for obtaining such composites, seeking in an intimate mixture of different constituents of the composite on a very fine scale – nanocomposites of NiO/C and Ni/NiO/C. This is in contrast with other methods, which usually involve physical mixing of components at some stage of composite formation. The two different composites have been characterized in detail and investigated subsequently through electrochemical analysis for their suitability as electrode materials for capacitors. The performance, especially of the Ni/NiO/C composite, is encouraging, indicating the usefulness of the "single-source" approach to the synthesis of carbonaceous composites.

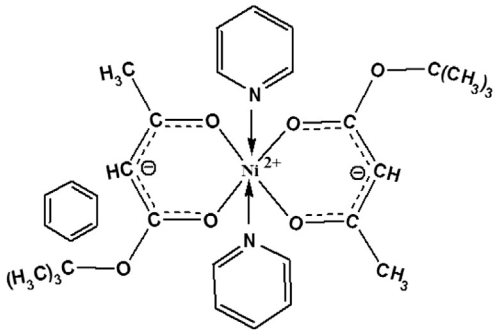

Fig. 1. Molecular structure of precursor $Ni(tbob)_2py$ used to synthesize NiO composites.

2. Experimental procedure

The choice of the precursor nickel complex was made assuming that the degree of incorporation of carbon into NiO derived from it (by the process detailed below) would be high if the proportion of carbon in the complex is high. One such complex is *tert*-butyl-3-oxobutanoate Ni(II) [designated $Ni(tbob)_2$], which has 32 mol% of carbon when adducted with pyridine and solvated with benzene. The complex was synthesized by the procedure reported previously by us [25] in a 30% aqueous ethanolic medium, using $Ni(NO_3)_2.9H_2O$ (SD Fine chemicals) as the metal source, tertiary butyl-3-oxobutanoate (Alfa Aesar) as the ligand, and pyridine (Merck) as the adduct. It was subsequently crystallized from benzene (Merck), whereupon crystals of bis *tert*-butyl-3-oxobutanoate Ni(II) dipyridine benzene solvate, [$Ni(tbob)_2py$], are formed (Fig. 1). The proportion of carbon in this solvate complex is 38 mol%.

NiO-containing products was synthesized by microwave irradiation of two different solutions of $Ni(tbob)_2py$ (1 g) – one in chloroform (45 ml) (SD Fine chemicals) and the other in ethylene glycol dimethyl ether (EGDME, 45 ml) (Merck). This choice of solvents was based on our previous approach to the synthesis of NiO and Ni/NiO through microwave irradiation [26]. To limit agglomeration of the resulting particles, an aqueous solution of the surfactant polyvinylpyrrolidone (PVP K-90, Rolex chemicals) (in 15 ml of water) was added to each reactant solution. (The aqueous part of the surfactant solution facilitates microwave absorption.) While the use of chloroform as the solvent was expected to yield a NiO-containing product [26], EGDME was chosen specifically to enhance reduction to metallic nickel. The consolidated solution of the complex and the surfactant was subjected to microwave irradiation in a domestic-type oven (2.45 GHz, 900 W) for 10 min. The solid precipitate so obtained centrifuged to obtain a powder, which was heated in air at 500 °C for 1 h to ensure that all remnant of the surfactant was removed. About 110 mg of final powder was obtained after annealing. Table 1 presents the details of experimental conditions employed in the syntheses.

X-ray powder diffraction (PANalytical, Cu-K_α radiation) was used to determine the crystallinity of the powder material and synthesized, to identify the phase(s), and to estimate the average size of the crystallites. Morphological analysis was carried out by

Table 1
Conditions employed in microwave-assisted synthesis of NiO composites.

Precursor (P)	Solvent	Surfactant (S)	P:S (w/w)	Solvent: H_2O (v/v)	Code
$Ni(tbob)_2py$	Chloroform	PVP K-90/H_2O	3:1	4:1	NiO/C
$Ni(tbob)_2py$	EGDME	PVP K-90/H_2O	3:1	4:1	Ni/NiO/C

field-emission scanning electron microscopy (FESEM, Zeiss Ultra55). Transmission electron microscopy (TEM, TECNAI F-30) was used to analyze the finer details of the morphology and the crystallinity of the powder material. Raman spectra were obtained using an argon ion laser (514 nm, Horiba Jobin-Yvon LabRAM HR 100). Core-level X-ray photoelectron spectra (XPS) of the synthesized powder material were collected on a Thermo Scientific Multilab-2000 instrument. Thermal stability of the powder materials was studied by thermogravimetric analysis (TA Instruments model STQ6000).

Electrodes were prepared by mixing 70 wt.% of the prepared composite powder with 20 wt.% of ketjen black and 10 wt.% of polyvinylidene fluoride (PVDF) as binder. To form electrodes, the mixture was applied on sand-blasted SS 316 substrates (measuring 10 mm × 10 mm) using *N*-methylpyrrolidone (NMP) solvent, and dried at 60 °C for 24 h. Each electrode contained 0.6 mg of the synthesized powder as active mass. All electrochemical measurements were made in a three-electrode configuration, wherein the composite coating on SS, the platinum foil, and the Ag/AgCl, Cl^- (3 M) electrode served, respectively, as the working, counter, and reference electrodes. Sodium sulfate (0.1 M) was used as the electrolyte. In addition, electrolyte-dependent electrochemical behavior was studied by using different electrolytes (KOH and $Ca(NO_3)_2 \cdot 4H_2O$). All the electrochemical measurements were conducted with an Autolab electrochemical instrument, model PGSTAT302N. Electrochemical impedance measurements were made on a Solartron Electrochemical Interface Model SI 1287.

3. Results and discussion

3.1. X-ray diffraction

The (annealed) powder material obtained from the two different synthesis protocols is black in color, hinting at the presence of carbon, as desired while choosing the precursor. The X-ray diffraction patterns of the annealed samples are shown in Fig. 2. It is clear from the diffraction patterns that the samples are crystalline, the broad peaks indicating that the grains present in the samples are very fine. The patterns can be indexed either to NiO or to a mixture of Ni and NiO, as shown (JCPDS File No. 00-004-0835 for NiO and 00-001-1258 for Ni). It is clear that use of chloroform as solvent results in phase-pure NiO, whereas the use of EGDME leads to the formation of both Ni and NiO – that is, a Ni/NiO composite.

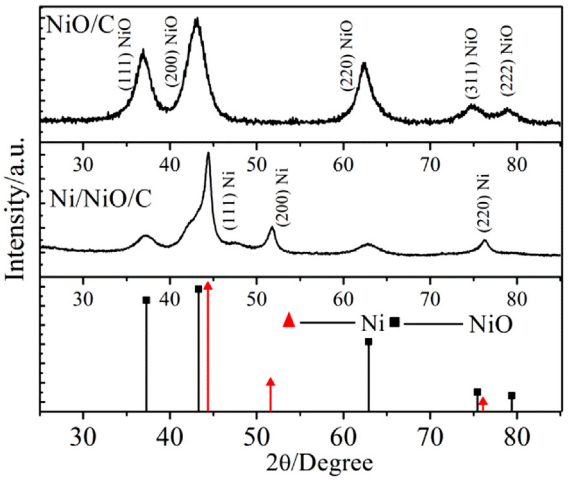

Fig. 2. XRD patterns of microwave-synthesized NiO/C and Ni/NiO/C, together with the standard (JCPDS) powder patterns for Ni and NiO.

The average crystallite size calculated using the Scherrer equation is 7 nm (considering the 111 reflection of NiO) for the NiO/C sample and 11 nm for the Ni/NiO/C composite (using the 200 reflection).

3.2. Raman spectroscopy

As the presence of carbon is expected in the reaction products, Raman spectra of the samples are obtained (Fig. 3). Four peaks located at about 469 cm^{-1}, 505 cm^{-1}, 690 cm^{-1} and 1060 cm^{-1} are observed in both the spectra. The first two peaks (469 cm^{-1} and 505 cm^{-1}) can be assigned, respectively, to the first-order transverse optical (TO) and longitudinal optical (LO) phonon modes of pure NiO [12,27,28]. The other two peaks (690 cm^{-1} and 1060 cm^{-1}) can be attributed to a combination of two TO and two LO modes of pure NiO. In addition to the features due to NiO, two broad peaks at 1341 cm^{-1} and 1601 cm^{-1} are observed in both the samples. These can be assigned to the presence of carbon in the samples. This carbon, present in the samples NiO/C and Ni/NiO/C, is graphitic in nature and nanometric in size. The peak at 1601 cm^{-1} is assignable to the graphitic G band, which is associated with the doubly degenerate in-plane transverse (iTO) and in-plane longitudinal optic (iLO) phonon modes (E_{2g} symmetry) arising from the first-order Raman scattering process. The peak at 1341 cm^{-1} is assigned to the graphitic D band, which involves one iTO phonon mode associated with the second-order Raman scattering process. The large FWHM of these "carbon peaks" indicates that the element is present in very fine particle size.

The Raman spectra, together with the XRD analysis, lead to the conclusion that the present microwave-assisted synthesis leads to the formation of the nanocomposites NiO/C and Ni/NiO/C, respectively, from chloroform and EGDME solutions. Thus, two different NiO-based nanocomposites, viz., NiO/C and Ni/NiO/C, can be obtained from the same adducted ketoesterate complex of nickel serving as the "single source". Such synthesis obviates the need for physical mixing, and provides homogeneity of composition on a fine scale, which results from the large density of nucleation in the solution medium under microwave irradiation.

3.3. Electron microscopy

The morphology of the samples can be discerned from the FE-SEM micrographs shown in Fig. 4. As seen from the micrographs

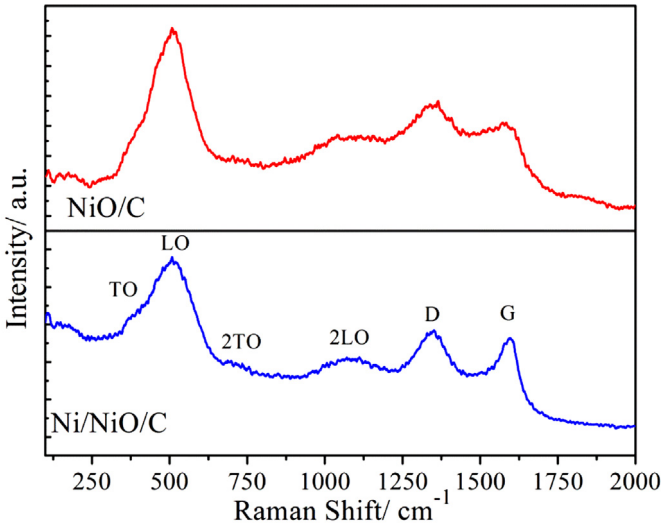

Fig. 3. Raman spectra of NiO-containing composites NiO/C and Ni/NiO/C, indicating the presence of oxide and carbon in both the samples.

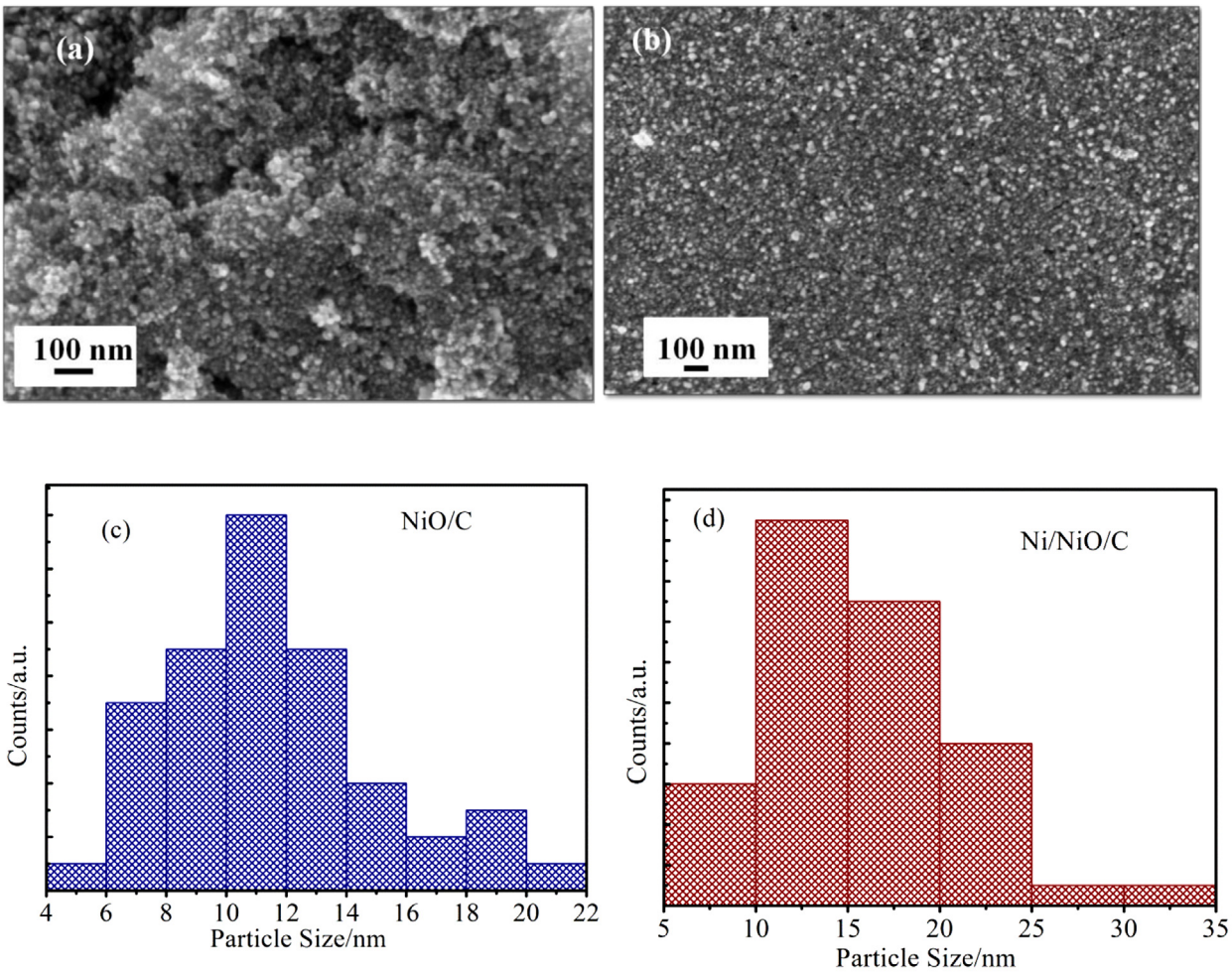

Fig. 4. FE-SEM images: spherical agglomerates of (a) NiO/C, (b) Ni/NiO/C; size distribution of these spherical entities, (c) NiO/C, (d) Ni/NiO/C.

(Fig. 4a and b), both the samples are similar in microstructure, i.e., they comprise spherical entities, which are uniformly distributed throughout. The size distribution of the particles in NiO/C and Ni/NiO/C is shown in Fig. 4c and d, indicating that particles within each sample are reasonably mono-disperse. The average diameter of these spherical entities is in the range of 10–20 nm, with some as small as 5 nm. Thus, the microwave-assisted solution synthesis technique can provide carbonaceous nanocomposites with a rather narrow particle size distribution.

The TEM images of both the composite samples NiO/C and Ni/NiO/C are shown in Fig. 5. While Fig. 5a and b shows low-resolution images, Fig. 5a′ and b′ shows high-resolution images of the samples. In the low-resolution images of NiO/C (Fig. 5a) and Ni/NiO/C (Fig. 5b), it can be seen that the particles are covered by a thin "coating" which may be an indication of a carbon layer present in both the composites. The particle size is deduced to be 8 nm and 12 nm for NiO/C and Ni/NiO/C, respectively. Well-resolved SAED ring patterns confirm the presence of NiO in NiO/C, and the mixed Ni/NiO composition in Ni/NiO/C. In the HRTEM, there can be seen a coating between the particles, without any clear fringe pattern, confirming that the particles are linked to each other through a thin layer of amorphous carbon, as evidenced by Raman analysis. Such a carbon layer is seen more clearly in Ni/NiO/C, which is synthesized under the reducing conditions, i.e., with ethylene glycol dimethyl ether as solvent (Fig. 5b′). Thus, in each sample, amorphous carbon is the "envelope" that encloses nanocrystalline NiO or a Ni/NiO composite, forming core/shell structures, where the shell is carbon and the composition of the core depends on the solvent employed.

3.4. X-ray photoelectron spectroscopy

XPS spectra of both the NiO-containing composite samples are shown in Fig. 6. As in other transition metal oxides, the XPS spectrum of NiO shows the most prominent inner shell NiO peaks and charge transfer shake-up satellites. The charge transfer between O 2p and Ni 3d is responsible for such shake-up features in the spectra [29–32]. As shown in the XPS spectrum of Fig. 6a, the Ni2p peak splits into two: $2p_{1/2}$ and $2p_{3/2}$. The $2p_{3/2}$ spectrum is fitted with two asymmetric Gaussian/Lorentzian components for the NiO surface. Upon fitting (Fig. 6c), the peak positions can be fixed at 855.6 eV and 853.7 eV.

It has been well established [29] that NiO is prone to adsorbing species like −OH, O_2^-, O_2^{2-}, O^- and H_2O on its surface. Hence, upon a careful fitting of the O 1s spectrum, it is found to resolve into three components (Fig. 6d) corresponding to the oxygen bonding modes with nickel and hydrogen: a water molecule (H–O–H) at 532.0–532.4 eV, a hydroxide (Ni–O–H) and/or NiOOH at 530.5–530.6 eV, and an oxide (Ni–O–Ni bond) at 529.3–529.8 eV. The details of the fitting of Ni $2p_{3/2}$ and O 1s features are given in Table 2. As shown in the table, there is a small but clear shift in binding energy of 0.2–0.4 eV from reported values. This shift may be accounted for by the incorporation of carbon into the oxide/

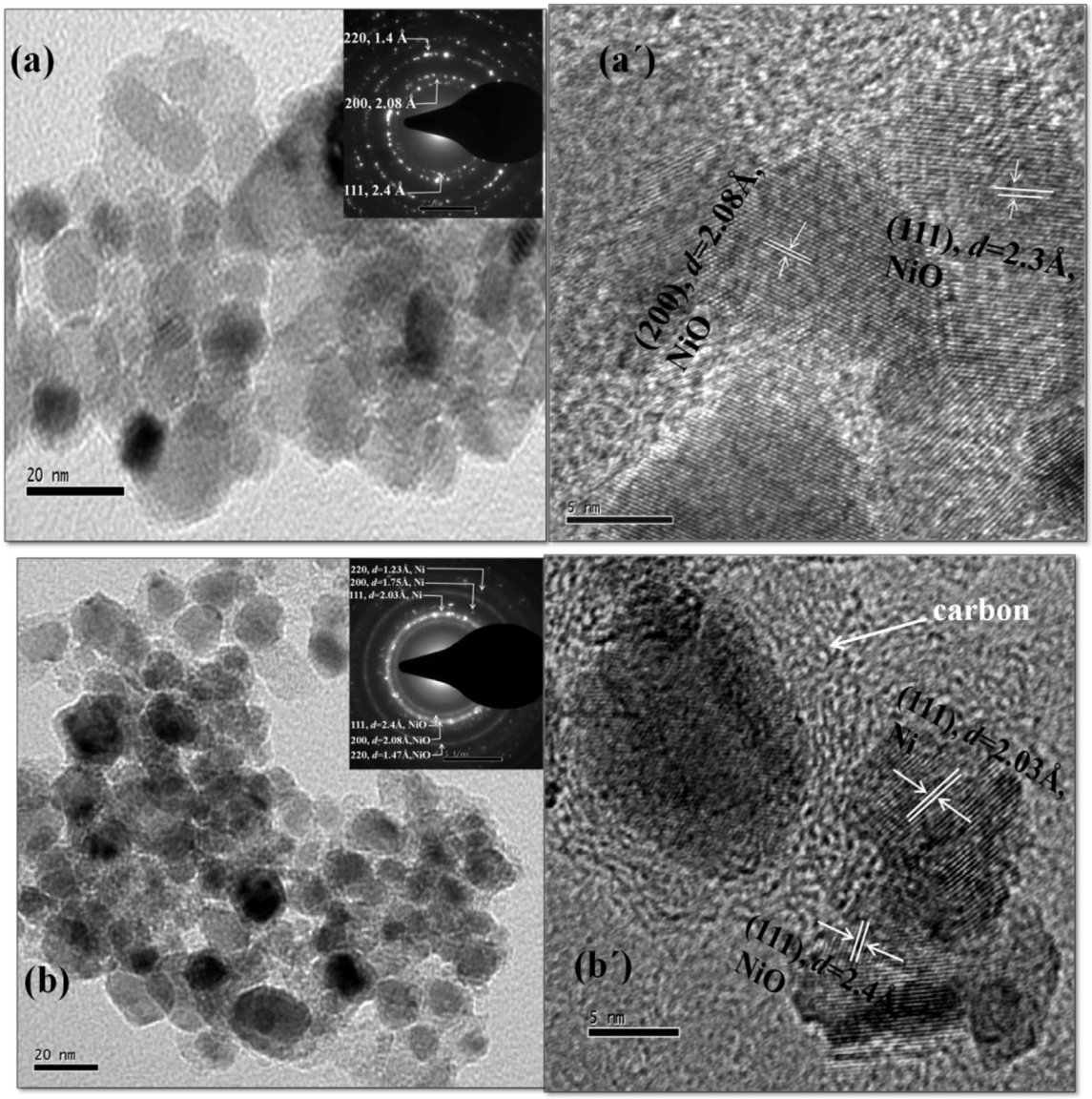

Fig. 5. FE-TEM images: dispersed nanoparticles of (a) NiO/C, (b) Ni/NiO/C composites; HRTEM images with clearly resolved fringes and thin carbon layer (a′) NiO/C, (b′) Ni/NiO/C. It is noteworthy that, in Ni/NiO/C, crystallites of Ni and NiO are within a couple of nanometers of each other.

composite matrix [33]. A careful examination of the C 1s spectrum can support such an observation more firmly (Fig. 6b). As shown in the C 1s spectrum, there is a variation in the peak shape and position, with asymmetry in peak shape in both the samples. Such asymmetry in the C 1s spectrum confirms the inferences drawn from the Raman spectra. Accordingly, such shifts in position in binding energy may be due to changes in the surface states caused by several moieties present in the samples NiO/C and Ni/NiO/C. The shifted positions in the C 1s spectrum are listed in Table 2, relative to the reported value of 284.2 eV.

3.5. Thermal analysis

The approximate composition of the composites is deduced through thermogravimetric analysis (TGA) conducted under ambient conditions, with airflow of 100 sccm and a heating rate of 5 °C min^{-1}. The sample mass taken during measurement is 10 mg in each case. The TGA data for the NiO/C and Ni/NiO/C composites are shown in Fig. 7. As evident from the figure, both the samples show a loss in weight at low temperature, presumably because of the loss of surface hydroxyl groups. Although the initial weight loss of sample Ni/NiO/C is “slow”, the loss is more “rapid” after the oxidation of metallic Ni, in a manner akin to the sample NiO/C. Above 400 °C, the rate of weight loss is moderate in both the samples. Between 400 and 700 °C, a maximum weight loss of 2.5% is observed, attributable to the loss of carbon present in the two composites. A similar finding has been reported previously in a different context, viz., in combustion-synthesized titania powder wherein a weight loss of 0.4% is observed in the 500–800 °C temperature range, and is attributed to the loss of carbon present in the sample [34].

The observed greater weight loss below 100 °C in the NiO/C sample is likely to be due to the weaker binding of the hydroxyl groups to the surface than in the Ni/NiO/C composite. In other words, the weight loss in Ni/NiO/C is due to the loss of surface hydroxyls, is hindered by surface modification due to carbon, which renders the release of hydroxyls more difficult. Such a difference is evidenced in the XPS spectra of the two samples. The weight loss in

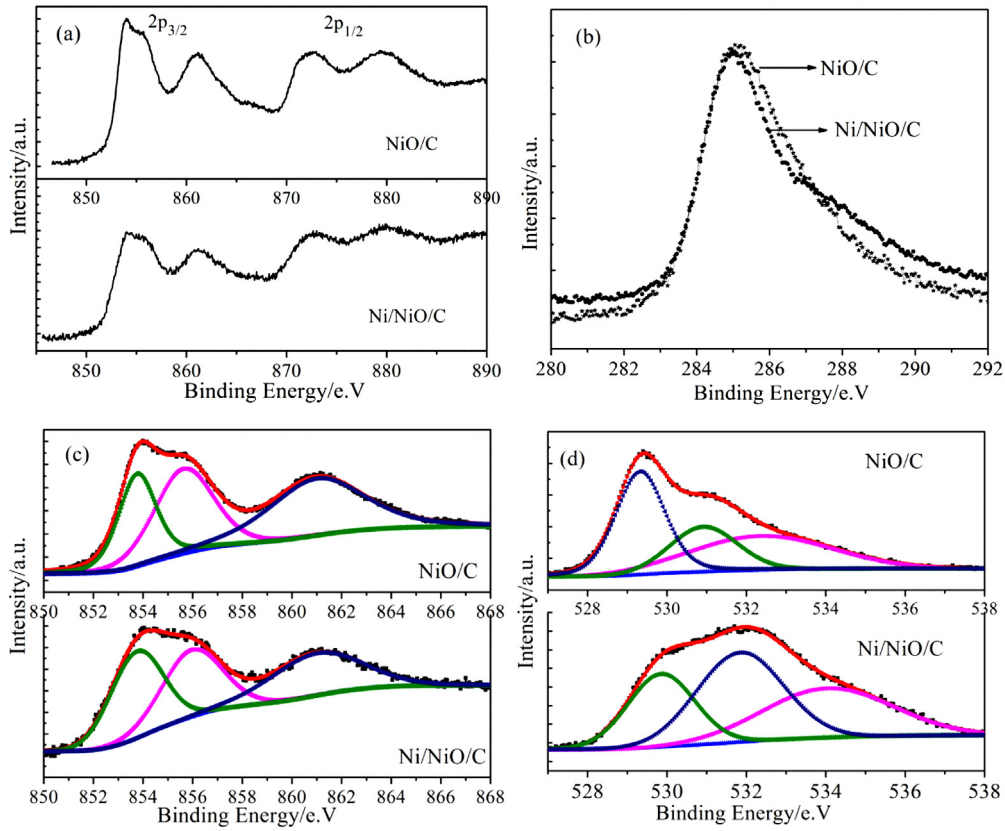

Fig. 6. XPS core level spectra of (a) Ni 2p showing intense shake up lines in both NiO/C and Ni/NiO/C samples, (b) highly asymmetric C 1s spectrum of NiO/C and Ni/NiO/C composites, (c) deconvoluted XPS spectrum for Ni $2p_{3/2}$, (d) deconvoluted XPS spectrum of O 1s.

NiO/C beyond 100 °C may be attributed entirely to the loss of elemental carbon. Assuming that no significant weight loss due to the oxidation of carbon occurs above 700 °C, the molar proportion of carbon in NiO/C is estimated from TGA to be ∼33%.

In the Ni/NiO/C composite, the weight gain between ∼250 °C and ∼350 °C (following the loss of surface hydroxyls) is attributable to the oxidation of metallic Ni to NiO. Noting (from the TGA data) that no significant loss of carbon (i.e., no significant weight loss) takes place up to ∼250 °C, and assuming that the weight gain between 250 °C and 350 °C is due to the oxidation of Ni, the proportion of Ni in the composite is estimated to be 25 mol%. Assuming that the weight loss between 350 °C and 700 °C is due to the oxidation of carbon, the proportion of carbon is estimated to be ∼55 mol%. Thus, the approximate molar composition of the Ni/NiO/C is 25:20:55.

3.6. Electrochemical characterization

3.6.1. Cyclic voltammetry

Cyclic voltammograms are recorded in 0.1 M Na_2SO_4 electrolyte at different scan rates in the range of 5–50 mV s^{-1}, within a potential window of 1 V (Fig. 8). Both the composites show voltammograms that are quite rectangular, with nearly mirror-image characteristics, indicating their suitability as electrode materials in capacitors. The rectangular nature of the voltammograms is more pronounced in samples synthesized under reducing conditions, i.e., Ni/NiO/C. Such behavior further establishes the Ni/NiO/C composite as promising electrode material. A linear rise of the cathodic current with scan rate indicates the capacitive nature of both the composite electrode materials (Fig. 8b). Further, the absence of redox peaks in the voltammograms indicates that the charge

Table 2
Peak positions (in eV) of Ni $2p_{3/2}$ and O 1s and C 1s calculated from XPS spectra.

Sample	Ni $2p_{3/2}$		O 1s			C 1s
			Ni–O–Ni	Ni–OH	H–O–H	
NiO/C	853.7	855.8	529.6	531.5	532.5	285.0
Ni/NiO/C	853.7	855.9	529.8	531.8	533.6	285.1

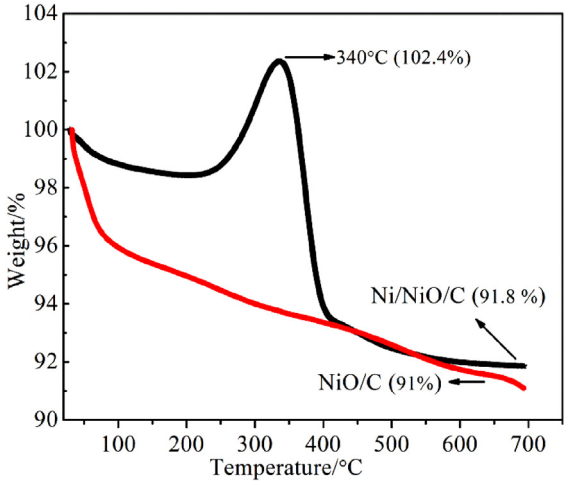

Fig. 7. TGA of NiO/C and Ni/NiO/C samples in air at a heating rate of 5 °C min^{-1}, evidencing metallic Ni from the "oxidation peak" and carbon from weight loss at higher temperatures.

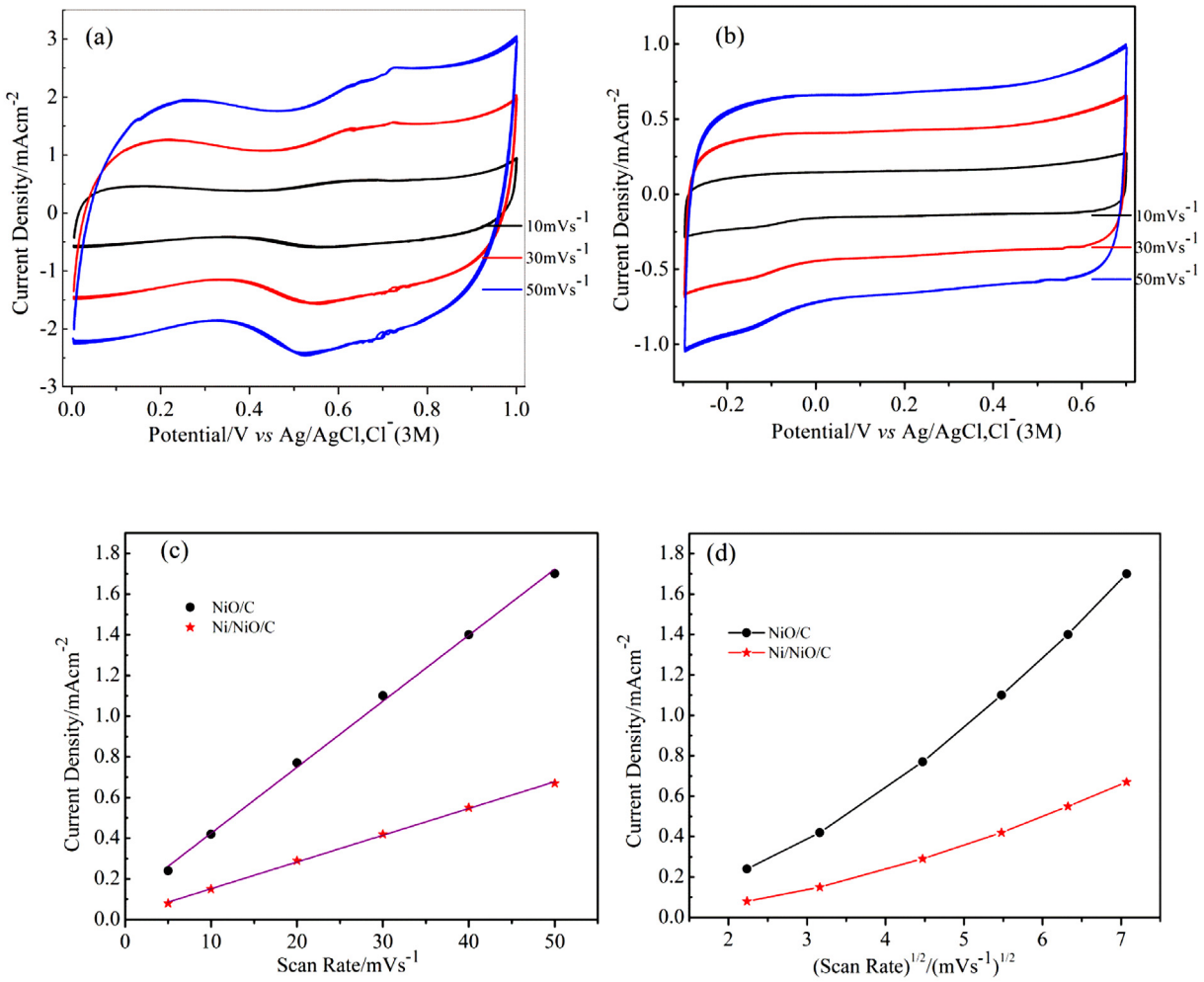

Fig. 8. Electrochemical behavior of NiO composite electrodes in 0.1 M Na_2SO_4 as electrolyte *vs.* Ag/AgCl, Cl^{-1} (3 M): cyclic voltammograms, (a) NiO/C, (b) Ni/NiO/C, (c) current *vs.* scan rate, (d) current *vs.* square root of scan rate.

storage mechanism is a surface process. The observed linearity of current versus scan rate (Fig. 8c) and nonlinearity in current versus of square root of scan rate (Fig. 8d) indicate that the electrode process follows a charge transfer-limited surface process, rather than a diffusion-controlled one.

3.6.2. *Galvanostatic charge/discharge cycling*

Charge/discharge cycling of both the composite electrodes is recorded within a potential window of 1 V, in 0.1 M Na_2SO_4 as electrolyte, at specific current of 0.5 A g^{-1} (Fig. 9). This shows a linear rise and fall in potential with time during charging/discharging, evidencing the capacitive nature of the electrodes. The mirror-image symmetry of these curves is verified over ten charge/discharge cycles, confirming the reversibility of the electrode processes. The specific capacitance (SC) of each electrode is calculated from the discharge curves using equation (1) and the values are listed in Table 3.

$$C_{sp} = (It)/(\Delta Vm) \quad (1)$$

where, I, t, ΔV and m are the discharge current, discharge time, potential window and the active mass of electrode material, respectively. Highest SC measured is 113 F g^{-1} for the Ni/NiO/C composite, which is comparable with the Ni/NiO composite [35]. For NiO/C composite the calculated SC is only 74 F g^{-1}.

As revealed by electron microscopy, both the NiO-containing composites have similar nanostructures, i.e., they comprise nearly spherical particles with particle size in the nanometer range. Thus, the difference between them in the measured SC may be attributed to their differing compositions. As reported earlier [35], electrode materials with poor conductivity hinder electronic and ionic conduction during charge/discharge cycling, resulting in degraded electrode performance. While the conductivity of nanometric NiO may be somewhat higher, significant enhancement in conductivity can be achieved by "additives" to NiO, such as metallic Ni and/or graphitic carbon, thus improving the capacitive behavior of NiO-based electrode material. Though the presence of metallic Ni modifies only the electrical conductivity in the samples, incorporating carbon in the oxide matrix adds the double-layer capacitive component to the inherent pseudocapacitive nature of oxide electrodes. Both of these capacitive mechanisms come together to yield the high specific capacitance measured in the Ni/NiO/C sample. This is affirmed by the almost perfectly rectangular shape of its voltammogram. Further, as listed in Table 3, the equivalent series resistance is greater in NiO/C than in Ni/NiO/C. Hence, the presence of metallic nickel and carbon in the matrix not only enhances the conductivity but also reduces the equivalent series resistance, leading to better electrode performance.

Rate capability of these electrodes is examined in 0.1 M Na_2SO_4 electrolyte at different current densities (Fig. 9b). As current density

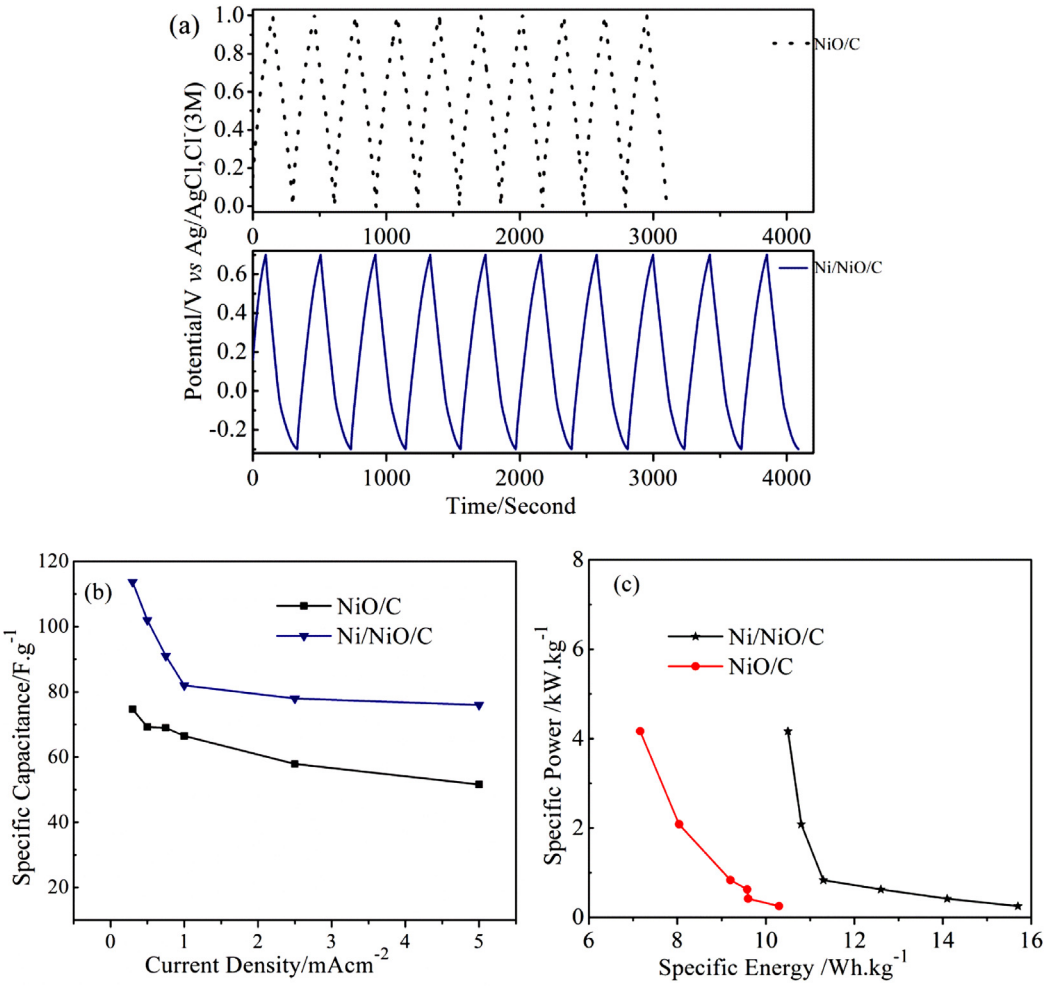

Fig. 9. Galvanostatic charge/discharge cycling (a) NiO/C and Ni/NiO/C in 0.1 M Na_2SO_4 as electrolyte at current density of 0.5 A g^{-1}, (b) variation of specific capacitance with current density and (c) Ragone plot showing variation of specific power and specific energy in 0.1 M Na_2SO_4 electrolyte.

is increased, the SC suffers an initial reduction, though it stabilizes at higher current densities. This is because, at higher current densities, the kinetics of charge transfer at the electrode/electrolyte interface is faster. As a result, not all the active mass of electrode material is used for the charge storage process, diminishing the specific capacitance.

Practical advantage of supercapacitors is that they have higher power densities than batteries and fuel cells. Hence, an evaluation of the energy and power densities of electrodes showing capacitive behavior is appropriate. As such, the specific power (SP) and specific energy (SE) of the electrodes, NiO/C and Ni/NiO/C are calculated using equations (2) and (3) and shown in Fig. 9c as a Ragone plot.

$$\text{Energy density} = (VIt)/2m \quad (2)$$

$$\text{Power density} = (VI)/2m \quad (3)$$

Table 3
Electrochemical characteristics of the NiO-based nanocomposites.

Sample	Average size in nm	Ohmic drop in Ω	Specific capacitance in F g^{-1}
NiO/C	8–15	46	74
Ni/NiO/C	10–15	23	113

A maximum specific power of 4.1 kW kg^{-1} is obtained at a current density of 5 mA cm^{-2}, corresponding to a specific energy of 7.1 W h kg^{-1} and 10.5 W h kg^{-1} for NiO/C and Ni/NiO/C, respectively.

3.6.3. Impedance analysis of nickel oxide composites

The electrochemical impedance spectra of the various samples are obtained at open circuit potential with an AC perturbation of 5 mV (Fig. 10a). The impedance spectra of all the samples follow a similar trend, i.e., they are composed of a semicircle at high frequencies and a linear part at the low-frequency end. The semicircle is associated with the surface properties of the composite electrode at high frequencies and corresponds to the Faradaic charge-transfer resistance (R_{ct}). The measured impedance spectra are analyzed and fitted using a standard model on the basis of the equivalent circuit given in Fig. 10b, where R_s is the solution resistance, W is the diffusion component and CPE is the constant phase element. As shown in Table 4, the fitted R_{ct} of NiO/C > R_{ct} of Ni/NiO/C. The lower R_{ct} value in the composite Ni/NiO/C is attributable to the presence of both carbon and metallic Ni in the sample. It is surmised that the percolation of Ni nanoparticles in carbon matrix lowers the net resistance of the material which, in turn, minimizes the equivalent series resistance (ESR), which comprises electrode resistance, electrolyte resistance, and resistance to the diffusion of ions in the electrode porosity. This ESR is inversely related to the power density.

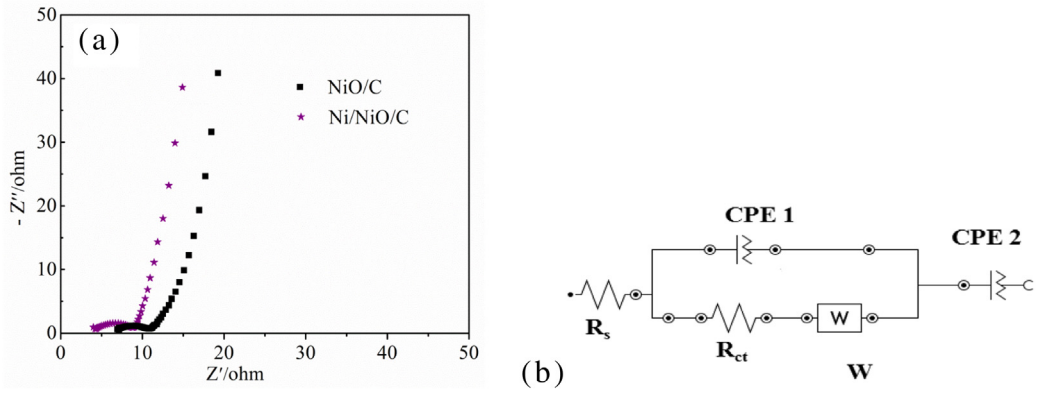

Fig. 10. (a) Electrochemical impedance spectra of NiO composite samples in 0.1 M Na_2SO_4 electrolyte and (b) fitted equivalent circuit.

3.6.4. Effect of electrolyte on the electrochemical behavior of Ni/NiO/C

As noted above, the charge storage mechanism of the NiO-containing composite electrode is the outcome of redox processes occurring at the electrode surface and the adsorption of ions into the active material. To examine the nature of interaction of ions at the electrode/electrolyte interface, the electrochemical analysis is extended to 0.1 M solution of $Ca(NO_3)_2 \cdot 4H_2O$ and KOH as electrolytes, separately. Cyclic voltammograms of the Ni/NiO/C sample are recorded at a potential window of 1 V, at sweep rates in the range of 5–50 mV s^{-1} (Fig. 11) in both the electrolytes. As with Na_2SO_4 as electrolyte, the voltammograms show ideal capacitive behavior, with quasi-rectangular shapes in both $Ca(NO_3)_2 \cdot 4H_2O$ (Fig. 11a) and KOH (Fig. 11b) electrolytes. Similar observations are made with MnO_2 electrodes in different electrolytes [36,37]. Furthermore, no

Table 4
R_s and R_{ct} values from fitted impedance data.

	R_s/ohm	R_{ct}/ohm
NiO/C	6.1	6.3
Ni/NiO/C	5.6	6.1

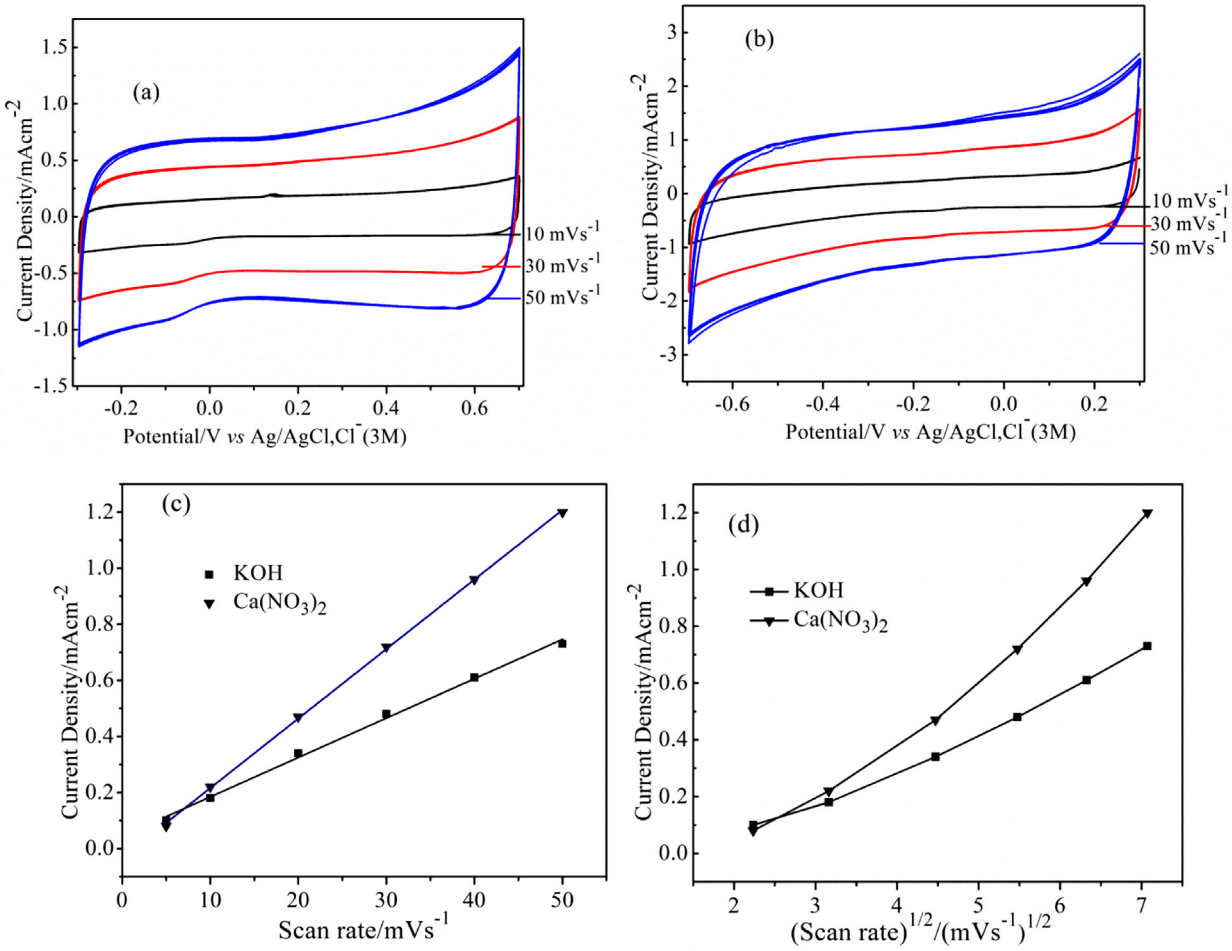

Fig. 11. Cyclic voltammogram of Ni/NiO/C in (a) 0.1 M $Ca(NO_3)_2$, (b) 0.1 M KOH, (c) linear rise in current with scan rate in $Ca(NO_3)_2$ and KOH and (d) current *vs.* square root of scan rate in $Ca(NO_3)_2$ and KOH electrolyte.

redox peaks appear within the selected potential window. The current associated with the voltammograms shows a linear rise, further confirming the capacitive nature of the oxide composite electrode (Fig. 11c). A non-linear rise in the cathodic current with the square root of scan rate confirms the charge transfer-controlled nature of the electrochemical process (Fig. 11d).

Charge/discharge cycles are recorded in 0.1 M $Ca(NO_3)_2{\cdot}4H_2O$ and KOH (Fig. 12a) in a potential window of 1 V. The capacitive nature of the electrodes is again ascertained through the linear rise in potential with time, which is an additional criterion for capacitive electrode materials. Extended cycles show retention of the mirror image character when $Ca(NO_3)_2{\cdot}4H_2O$ is used as the electrolyte (Fig. 12a). The specific capacitance (SC) calculated using equation (1) is found to be 143 F g^{-1} for the Ni/NiO/C sample with 0.1 M $Ca(NO_3)_2{\cdot}4H_2O$ as electrolyte, at a specific current of 0.5 A g^{-1}. The SC is calculated for the KOH as electrolyte is 97 F g^{-1}, at a specific current of 1 A g^{-1} (Fig. 12b).

As reported earlier [37], polyvalent cations are preferred in studying capacitive behavior, as each ion intercalated into the host compound results in a concurrent charge transfer of more than one electron to the host material. Hence, the SC increases, because the capacity is purely dependent on the redox process at the electrode/electrolyte interface and is determined by the number of intercalated ions participating in the charge transfer event.

The measured higher capacity of Ni/NiO/C in $Ca(NO_3)_2{\cdot}4H_2O$ can be explained on the basis of ionic radii and the charge transfer process occurring at the electrode/electrolyte interface. At the interface, adsorption sites being the same, charge due to adsorbed Ca^{2+} ($r^{2+}_{Ca} = 1.14$ Å) ions is greater than that due to adsorbed Na^+ ions ($r_{Na^+} = 1.16$ Å) and K^+ ($r_{K^+} = 1.38$ Å), thus accounting for the increase in SC.

3.6.5. Stability of Ni/NiO/C electrode in Na_2SO_4, $Ca(NO_3)_2{\cdot}4H_2O$, and KOH electrolytes

Long-term cycle stability is an essential requirement for an electrode material if it is to be utilized in practice. The stability of the Ni/NiO/C sample is evaluated by repeating the galvanostatic charge/discharge cycling in 0.1 M Na_2SO_4, 0.1 M $Ca(NO_3)_2{\cdot}4H_2O$, and 0.1 M KOH electrolytes, *vs.* Ag/AgCl, Cl^- (3 M) reference electrode, within a potential range of 1 V. A specific current of 1 A g^{-1} in KOH and 0.5 A g^{-1} in Na_2SO_4 and $Ca(NO_3)_2{\cdot}4H_2O$, is applied during the cyclability test conducted for 1000 cycles (Fig. 13). The electrodes show reliable stability over the 1000 cycles,

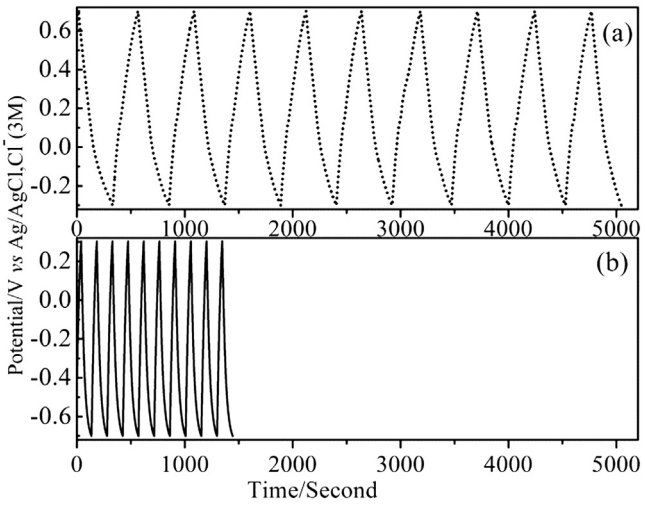

Fig. 12. Charge/discharge cycling of Ni/NiO/C in 0.1 M (a) $Ca(NO_3)_2{\cdot}4H_2O$ and (b) KOH.

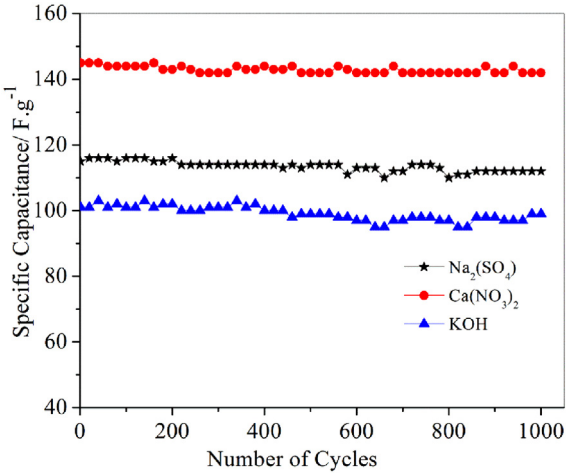

Fig. 13. Cycle stability of Ni/NiO/C composite in 0.1 M solution of Na_2SO_4, $Ca(NO_3)_2{\cdot}4H_2O$ and KOH.

in each electrolyte. The SC fluctuates by about 5 F g^{-1} in KOH electrolyte, whereas the fluctuation is limited to 2 F g^{-1} when either Na_2SO_4 or $Ca(NO_3)_2{\cdot}4H_2O$ is the electrolyte. The Faradaic efficiency calculated is 97%, confirming the potential utility of the NiO-containing nanocomposite electrode materials.

4. Conclusions

Nanometric carbonaceous nickel oxide-based composites are synthesized via microwave-assisted rapid chemical route, using a "single source" adducted β-ketoesterate complex of nickel. Through proper choice of reaction conditions, two different composite materials, viz., NiO/C and Ni/NiO/C, can be synthesized. The low electrical conductivity of pure nickel oxide is thus compensated for by incorporating metallic nickel and/or carbon, rendering the composites suitable for capacitor electrodes. The formation of composites in a single-step process from a single chemical source results in compositional homogeneity on a fine scale. Electrochemical measurements show that these composites are excellent electrode materials for capacitors, with the presence of metallic nickel leading to lower series resistance in the Ni/NiO/C material. Electrolyte-dependent electrochemical behavior is also studied, to obtain a promising specific capacitance, viz., 113 F g^{-1} in 0.1 M Na_2SO_4 and 143 F g^{-1} in $Ca(NO_3)_2{\cdot}4H_2O$.

Acknowledgments

The authors thank NPMASS for funding this effort and CeNSE-IISc, INI-IISc and IISc Surface Science Facility for providing access to various characterization techniques.

References

[1] D. Wang, R. Xu, X. Wang, Y. Li, Nanotechnology 17 (2006) 979.
[2] J. He, H. Lindstrom, A. Hagfeldt, S. Lindquist, J. Phys. Chem. B 103 (1999) 8940.
[3] Z. Yue, W. Niu, W. Zhang, G. Liu, W.J. Parak, J. Colloid Interface Sci. 348 (2010) 227.
[4] M.M. Uplane, S.H. Mujawar, A.I. Inamdar, P.S. Shinde, A.C. Sonavane, P.S. Patil, Appl. Surf. Sci. 253 (2007) 9365.
[5] S.H. Lee, C.E. Tracy, J. Roland Pitts, Electrochem. Solid-State Lett. 7 (2004) A299.
[6] X. Wang, J. Song, L. Gao, J. Jin, H. Zheng, Z. Zhang, Nanotechnology 16 (2005) 37.
[7] K. Liang, X. Tang, W. Hu, J. Mater. Chem. 22 (2012) 11062.
[8] X. Li, A. Dhanabalan, C. Wang, J. Power Sources 196 (2011) 9625.

[9] N. Chopra, W. Shi, A. Bansal, Carbon 49 (2011) 3645.
[10] K. Lota, A. Sierczynska, G. Lota, Int. J. Electrochem. 2011 (2011) 1.
[11] H.C. Chang, H.Y. Chang, W.J. Su, K.Y. Lee, W.C. Shih, Appl. Surf. Sci. 258 (2012) 8599.
[12] Y. Xia, W. Zhang, Z. Xiao, H. Huang, H. Zeng, X. Chen, F. Chen, Y. Gan, X. Tao, J. Mater. Chem. 22 (2012) 9209.
[13] H. Li, Y. Li, R. Wang, R. Cao, J. Alloy Compd. 481 (2009) 100.
[14] E. Frackowiak, F. Beguin, Carbon 39 (2001) 937.
[15] C. Du, N. Pan, J. Power Sources 160 (2006) 1487.
[16] A.G. Pandolfo, A.F. Hollenkamp, J. Power Sources 157 (2006) 11.
[17] Y. Wang, Z. Shi, Y. Huang, Y. Ma, C. Wang, M. Chen, Y. Chen, J. Phys. Chem. C 113 (2009) 13103.
[18] J.M. Miller, J. Electrochem. Soc. 144 (1997) L309.
[19] C. Yuan, X. Zhang, L. Su, B. Gao, L. Shen, J. Mater. Chem. 19 (2009) 5772.
[20] L. Yuan, X.-H. Lu, X. Xiao, T. Zhai, J. Dai, F. Zhang, B. Hu, X. Wang, L. Gong, J. Chen, C. Hu, Y. Tong, J. Zhou, Z.L. Wang, ACS Nano 6 (2012) 656.
[21] E. Frackowiak, V. Khomenko, K. Jurewicz, K. Lota, F. Beguin, J. Power Sources 153 (2006) 413.
[22] S.K. Meher, P. Justin, G.R. Rao, ACS Appl. Mater. Interfaces 3 (2011) 2063.
[23] C. Parada, E. Moran, Chem. Mater. (2006) 2719.
[24] N. Behm, D. Brokaw, C. Overson, D. Peloquin, J.C. Poler, J. Mater. Sci. 48 (2012) 1711.
[25] S.K. Nayak, A. Jena, G.M. Neelgund, S.A. Shivashankar, T.N. Guru Row, Acta Crystallogr. E 63 (2007) m1604.
[26] A. Jena, N. Munichandraiah, S.A. Shivashankar, MRS Proc. 1406 (2012). mrsf11.
[27] G. Katumba, B.W. Mwakikunga, T.R. Mothibinyane, Nanoscale Res. Lett. 3 (2008) 421.
[28] X. Ni, Q. Zhao, F. Zhou, H. Zheng, J. Cheng, B. Li, J. Cryst. Growth 289 (2006) 299.
[29] A. Berlich, Y.C. Liu, H. Morgner, Radiat. Phys. Chem. 74 (2005) 201.
[30] A. Berlich, Y.C. Liu, H. Morgner, Surf. Sci. 602 (2008) 3737.
[31] M. Chigane, M. Ishikawa, J. Chem. Soc. Faraday Trans. 94 (1998) 3665.
[32] B.P. Payne, M.C. Biesinger, N.S. McIntyre, J. Electron. Spectrosc. 175 (2009) 55.
[33] G.E. Haslam, K. Sato, T. Mizokawa, X.Y. Chin, G.T. Burstein, Appl. Phys. Lett. 100 (2012) 231601.
[34] K. Nagaveni, M.S. Hegde, N. Ravishankar, G.N. Subbanna, G. Madras, Langmuir 20 (2004) 2900.
[35] J.H. Kim, S.H. Kang, K. Zhu, J.Y. Kim, N.R. Neale, A.J. Frank, Chem. Commun. 47 (2011) 5214.
[36] P.K. Nayak, N. Munichandraiah, J. Electroanal. Chem. 685 (2012) 37.
[37] C. Xu, H. Du, B. Li, F. Kang, Y. Zeng, J. Electrochem. Soc. 156 (2009) A73.